


Catalytic Behavior and In Situ X-Ray Diffraction of Promoted Iron Catalysts for Fischer-Tropsch Synthesis

Ruoxi Wen*, Johannes Thiessen, and Andreas Jess

DOI: 10.1002/cite.202200056

 This is an open access article under the terms of the Creative Commons Attribution License, which permits use, distribution and reproduction in any medium, provided the original work is properly cited.



Supporting Information
available online

The effects of structural promoters (ZnO, SiO₂, and Al₂O₃) on the phase transformation during reduction and Fischer-Tropsch synthesis (FTS) of a FeCuK catalyst were investigated by in situ X-ray diffraction and the FTS catalytic performance was studied in a fixed-bed reactor. The reduction follows the path of Fe₂O₃/K₂Fe₂₂O₃₄ → Fe₃O₄ → α-Fe. The addition of ZnO, SiO₂, and Al₂O₃ delayed and prolonged the reduction. The iron carbides formed under reaction conditions were χ-Fe₅C₂ and ε-Fe₂C. The presence of ZnO, SiO₂, and Al₂O₃ favored the formation of χ-Fe₅C₂. ε-Fe₂C is a more active phase. Besides, ε-Fe₂C seems to favor the formation of CO₂ and C₅₊ and χ-Fe₅C₂ benefits CH₄ and C₂–C₄ products.

Keywords: Fischer-Tropsch synthesis, In situ X-ray diffraction, Iron phases

Received: May 13, 2022; *revised:* September 06, 2022; *accepted:* September 13, 2022

1 Introduction

Fischer-Tropsch synthesis (FTS) is an important process for producing chemicals and fuels from coal, natural gas, biomass, or even from renewable hydrogen and CO/CO₂. FTS is a heterogeneous catalytic reaction that converts CO and H₂ (syngas) into hydrocarbons like gasoline, diesel oil, waxes [1]. Cobalt- and iron-based catalysts are commercially used catalysts [2]. Compared to cobalt-based catalysts, iron-based catalysts have the advantages of low cost and lower sensitivity towards poisons. Besides, iron also possesses a high activity for CO₂ via the water gas shift (WGS) reaction, which makes them particularly suitable for syngas low in hydrogen, e.g., feedstocks such as coal and biomass are used [2, 3]. Commonly, either precipitated iron or molten iron catalysts are utilized for low-temperature and high-temperature FTS, respectively [2]. Sintered iron catalysts are barely mentioned in the literature. Frohning et al. [4] reported about a sintered iron catalyst, which favors formation of gasoline and diesel even at low temperatures.

To improve the performance of iron catalysts, various metal/metal oxide promoters are added. There are mainly three categories. Firstly, reduction promoters are used to increase the reducibility of iron oxides, which are inactive or less active for the FTS [5, 6]. Copper, the mainly applied reduction promoter, not only accelerates the reduction rate of Fe₂O₃ to Fe₃O₄ [7, 8], but also has a positive effect on the FTS activity [7, 9, 10]. Secondly, alkali promoters are used as

electronic promoters to increase FTS activity, olefin and long-chain hydrocarbon selectivities [11]. Compared with other alkali promoters, due to its low price and good performance, potassium is considered as the best alkali promoter [5, 12, 13]. The last category are structural promoters, which are used to increase the dispersion and physical attrition of iron catalysts, e.g., SiO₂, Al₂O₃, and ZnO [10, 14–18]. The effects of different promoters on the catalytic performance of FTS have been thoroughly studied in the literature. However, it is known that iron-based catalysts undergo phase changes and a variety of iron carbide phases can form under reaction conditions (syngas atmosphere). Until now it is not clear how exactly the different structural promoters such as, ZnO, SiO₂, and Al₂O₃ influence the iron phase transformation under reduction and reaction conditions of FTS and how phases correspond with the FTS catalytic performance.

In this work, sintered iron catalysts promoted with Cu and K and different structural promoters (ZnO, SiO₂, and Al₂O₃) are used to investigate the effects of these structural

Ruoxi Wen, Dr.-Ing. Johannes Thiessen,
Prof. Dr.-Ing. Andreas Jess
ruoxi.wen@uni-bayreuth.de
University of Bayreuth, Department of Chemical Engineering,
Center of Energy Technology, Universitätsstraße 30, 95447 Bay-
reuth, Germany.

promoters on the phase transformation during reduction (12 % H₂ in N₂ → H₂, 350 °C) and under FT reaction conditions (H₂/CO = 2:1, 220 °C, 9 bar) by using in situ X-ray diffraction (XRD). The composition of the iron species was measured during the reduction and FTS reaction to illustrate the effect of ZnO, SiO₂, and Al₂O₃ of the promoted catalysts. In addition, the FTS catalytic performance of all catalysts was studied in a fixed-bed reactor at the same conditions as for the in situ XRD to correlate the catalyst composition with its activity and selectivity.

2 Experimental Section

2.1 Catalyst Preparation

The different promoted catalysts used in this study are sintered iron catalysts, which were prepared by a method following the procedure found in [4]. In brief, 40 g of metal oxide powders were mixed and the mixtures were ball-milled (Pulverisette 5) at 400 rpm for 30 min (6 times 5 min ball milling with 20 min pause in between) in a ZrO₂ crucible along with 60 ZrO₂ balls of 10 mm in diameter and then dried at room temperature. Thereafter, potassium carbonate and water were mixed with the ground powder and water was removed again by drying in an oven at 110 °C. The dried powders were sintered in a muffle furnace by heating to 1100 °C at 10 °C min⁻¹ and then holding at that temperature for 90 min. The obtained samples were crushed and sieved into 212- to 250-μm particles. Depending on the type and amount of promoters, the different promoted iron-based catalysts were designated as 100Fe15Cu5K, 100Fe15Cu5K5Zn, 100Fe15Cu5K12Si, and 100Fe15Cu5K12Al. The numbers are the weight ratio between the metal elements.

2.2 Catalyst Characterization

The composition of the fresh catalysts was determined by inductively coupled plasma optical emission spectroscopy (ICP-OES, Optima 7300 DV, PerkinElmer). The catalysts (0.11 g) with 8 mL of aqua regia (HCl/HNO₃ = 3:1) were added into the Teflon vessel. The samples were digested in a closed high pressure microwave-assisted oven (Multiwave 3000, Anton Paar). Afterwards, the samples were first diluted to 50 mL with deionized water and then further diluted 100 times with 2 % HNO₃ before they were measured with ICP-OES. The surface area of the fresh catalyst was measured by N₂ adsorption at -196 °C (Micromeritics Gemini V) and evaluated by the BET method in the pressure range of 5–30 % *p/p*₀. The samples (about 1 g) were degassed at 100 °C for 16 h prior to measuring. The BET surface area of the reduced catalysts was measured dynamically by single-point BET at -196 °C with 30 % N₂ in He after a reduction process analogous to the reduction prior to catalyst testing (Micromeritics AutoChem II).

2.3 In Situ X-Ray Diffraction

The reduction and FTS reaction were carried out in an Anton Paar XRK 900 reaction chamber, which is placed inside the goniometer circle of an X-ray diffractometer (Bruker D8 Advance), that can be heated up to 900 °C and pressurized to 10 bar. The phase composition and the X-ray diffractograms of the catalysts were thus measured in situ with CuKα radiation. The catalysts (about 300 mg) were loaded in the chamber and heated from 30 to 350 °C with 2 °C min⁻¹ under 12 % H₂ in N₂ (5 L_{STP}h⁻¹) and held for 2 h at 350 °C. Then, the gas composition was changed to pure H₂ for another 15 h at 350 °C (except for 100Fe15Cu5K12Al, which was held longer for 33 h in pure H₂ at 350 °C). At the end of the reduction, the catalysts were cooled to 30 °C. The X-ray diffractograms in a 2θ range of 32.9 to 61° with a scanning rate of 1.83° min⁻¹ were recorded at 30, 100, 150, 200, 250, 300, and 350 °C during the heating, continuously at 350 °C, and in the end at 30 °C. The reduced catalysts were then heated from 30 to 220 °C with 7.5 °C min⁻¹ under 4.5 L_{STP}h⁻¹ syngas flow at 9 bar (H₂/CO = 2:1 (v/v)) in the XRK 900 chamber. The X-ray diffractograms were taken in a 2θ range of 33 to 80° with a scanning rate of 0.77° min⁻¹ during the reaction. The phase composition and crystallite sizes during the reduction and FTS were determined by Rietveld refinement of the diffractograms using TOPAS 5 (Bruker AXS).

2.4 Evaluation of Activity and Selectivity of the Catalysts

The FTS catalytic performance was measured in a lab-scale reactor setup shown in Fig. S1 in the Supporting Information. The stainless steel fixed-bed reactor has an inner diameter of 1.4 cm. The reactor is surrounded by an aluminum block (diameter 12 cm) to ensure isothermal conditions. The bed temperature is controlled by an electrical heating jacket. All gas flows (H₂, CO, N₂, and a mixture of 1 % cyclopropane in N₂ used as internal standard for the analysis by online gas chromatography (GC)) are regulated by mass flow controllers. The total pressure is regulated by a back-pressure regulator. About 7.5 g iron-based catalyst diluted with sand (210–300 μm) was loaded into the reactor tube for each experiment. The catalysts were reduced with the same gas flow composition (20 L_{STP}h⁻¹) and the same heating ramp as described before for the reduction in the XRK 900 chamber. After cooling to 30 °C, the reactor was pressurized to reaction pressure (9 bar) under syngas (H₂/CO = 2:1 (v/v)) and then slowly heated to reaction temperature (220 °C). The syngas flow rate was typically 20 L_{STP}h⁻¹.

The volume flow was measured by a flow meter and the CO, H₂, and CO₂ concentrations were measured by a gas analyzer at the reactor outlet to calculate the conversion of CO and H₂ and CO₂ selectivity. Once the reaction temperature was reached, the online GC started to take samples every 4 h. The samples taken from cooling traps were analyzed via an offline GC.

The reaction rate was calculated by Eq. (1).

$$r = \frac{\dot{n}_{\text{CO,in}} - \dot{n}_{\text{CO,out}}}{m_{\text{Fe}}} \quad (1)$$

The selectivity for CO₂ is given by:

$$S_{\text{CO}_2} = \frac{\dot{n}_{\text{CO}_2,\text{out}}}{\dot{n}_{\text{CO,in}} - \dot{n}_{\text{CO,out}}} \quad (2)$$

The selectivity of hydrocarbon products was calculated by Eqs. (3) and (4).

$$S_{\text{C}_n} = \frac{\dot{m}_{\text{C}_n}}{\dot{m}_{\text{C}\rightarrow\text{CO,in}} - \dot{m}_{\text{C}\rightarrow\text{CO,out}} - \dot{m}_{\text{C}\rightarrow\text{CO}_2,\text{out}}} \quad (n = 1, 2, 3, 4) \quad (3)$$

$$S_{\text{C}_{5+}} = 1 - S_{\text{CH}_4} - S_{\text{C}_2} - S_{\text{C}_3} - S_{\text{C}_4} \quad (4)$$

3 Results and Discussion

3.1 Catalyst Characterization

The BET surface area of fresh and reduced catalysts, Fe⁰ crystallite size in the reduced catalyst, and different metal contents of the fresh catalyst are shown in Tab. 1. The BET surface area of the fresh catalyst, determined by multi-point BET measurement, shows that all catalysts have a relatively low surface area, which is due to the high sintering temperature during the catalyst preparation. After reduction, the surface area of most catalysts was higher than prior to reduction. Only the Zn-containing catalyst had a slightly reduced area. It should be noted that the given surface area is normalized to the mass of the fresh catalyst in both cases. In the reduced catalysts, 100Fe15Cu5K and 100Fe15Cu5K5Zn have a Fe⁰ crystallite diameter of 44 nm,

which is larger than the Fe⁰ particle diameter of 100Fe15Cu5K12Si and 100Fe15Cu5K12Al. The metal compositions of the fresh catalysts were determined by ICP-OES characterization.

The XRD patterns of the fresh catalysts are shown in Fig. 1. For 100Fe15Cu5K12Si and 100Fe15Cu5K12Al, only characteristic XRD patterns of Fe₂O₃ and Fe₃O₄ were identified. For the catalysts 100Fe15Cu5K and 100Fe15Cu5K5Zn, apart from Fe₂O₃ and Fe₃O₄, K₂Fe₂₂O₃₄

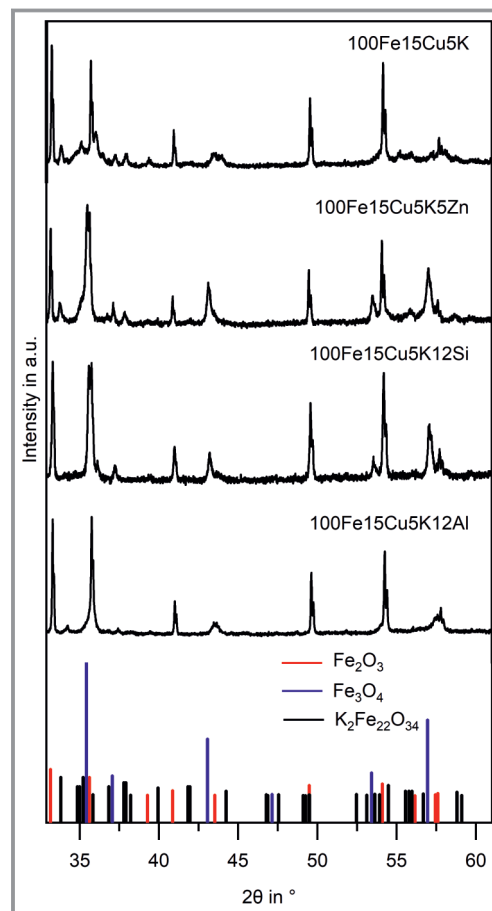


Figure 1. X-ray diffractograms of the fresh iron-based catalysts. The PDF card numbers are: Fe₂O₃ (00-033-0664), Fe₃O₄ (01-086-1362), K₂Fe₂₂O₃₄ (00-031-1034).

Table 1. BET surface area of fresh and reduced catalysts, Fe⁰ crystallite size in reduced catalysts and composition of fresh catalysts.

Catalyst	BET surface area [m ² g ⁻¹]		Fe ⁰ crystallite size ^{b)} in reduced catalyst [nm]	Mass ratios Fe/Cu/K/X (X= Zn, Si, Al)
	Fresh catalyst	Reduced catalyst ^{a)}		
100Fe15Cu5K	3.0	3.8	44	100:14.8:5.0
100Fe15Cu5K5Zn	4.4	3.5	44	100:15.4:5.4:5.2
100Fe15Cu5K12Si	0.2	8.3	33	100:15.1:5.5:–
100Fe15Cu5K12Al	2.2	10.4	13	100:16.8:4.7:11.4

a) Surface area of reduced catalyst by single-point measurement; b) data from the Rietveld refinement of the X-ray diffractogram of the reduced catalyst.

characteristic patterns were also observed. Diffraction patterns corresponding to CuO, ZnO, SiO₂, and Al₂O₃ were not observed in any catalyst, which indicates that the main bulk phase consists of iron oxides and other metals are dissolved in the lattice.

3.2 In Situ X-Ray Diffraction of the Reduction Process

The phase transformation of all iron-based catalysts during reduction was investigated using in situ XRD; the results during reduction are shown in Fig. 2. The specific reduction times of the iron species determined by in situ XRD are given in Tab. 2. During reduction, all the catalysts show two characteristic reflexes at 2θ of 43.3 and 50.4° emerging after reaching 250 °C, corresponding to metallic Cu. For the catalyst 100Fe15Cu5K, Fe₂O₃ started to reduce to Fe₃O₄ at 250 °C and was fully reduced to Fe₃O₄ at 350 °C after 3 h of reduction. For 100Fe15Cu5K5Zn and 100Fe15Cu5K12Al catalysts, Fe₂O₃ started to reduce to Fe₃O₄ at 300 °C and was fully reduced to Fe₃O₄ at 350 °C after 2.7 h and 3 h of the reduction process, respectively. For the 100Fe15Cu5K12Si catalyst, Fe₂O₃ started to reduce to Fe₃O₄ at 350 °C and was fully reduced to Fe₃O₄ after 5.5 h.

Table 2. Reduction time of different iron species monitored by in situ XRD.

Catalyst	t1 [h] ^{a)}	t2 [h] ^{b)}	t3 [h] ^{c)}	t4 [h] ^{d)}
100Fe15Cu5K	3.0	4.5	3.0	6.5
100Fe15Cu5K5Zn	2.7	4.5	4.5	8.6
100Fe15Cu5K12Si	5.5	4.5	3.7	6.8
100Fe15Cu5K12Al	3.0	4.5	5.0	–

a) Time at which Fe₂O₃ is fully reduced; b) time for gas change from 12 % H₂ in N₂ to 100 % H₂; c) time at which α -Fe starts to form; d) time at which all the iron oxides are fully reduced to α -Fe.

This shows that all the structural promoters (ZnO, SiO₂, and Al₂O₃) postpone the reduction process of Fe₂O₃ to Fe₃O₄. Besides, SiO₂ also prolongs the reduction process of Fe₂O₃ to Fe₃O₄.

During the reduction of 100Fe15Cu5K, α -Fe started to emerge after 3 h and was the only iron phase in the catalyst after 6.5 h. For the catalysts 100Fe15Cu5K5Zn and 100Fe15Cu5K12Si, α -Fe appeared after 4.5 and 3.7 h of reduction and the catalysts were fully reduced after 8.6 and 6.8 h, respectively. For the 100Fe15Cu5K12Al catalyst, α -Fe merged after 5 h, however, after 37 h of reduction, Fe₃O₄ was still not fully reduced to α -Fe, probably due to the formation of FeAl₂O₄. Fe₃O₄ and FeAl₂O₄ have the same crystal structure with a minimal difference in the lattice constant, and thus cannot be distinguished in the diffractograms. The different formation time of α -Fe and the time to full reduction show that all the structural promoters (ZnO, SiO₂, and Al₂O₃) delay and decelerate the reduction process of Fe₃O₄ to α -Fe. During the reduction of all catalysts, no FeO phase was observed and the reduction followed the process of Fe₂O₃/K₂Fe₂₂O₃₄ → Fe₃O₄ → α -Fe.

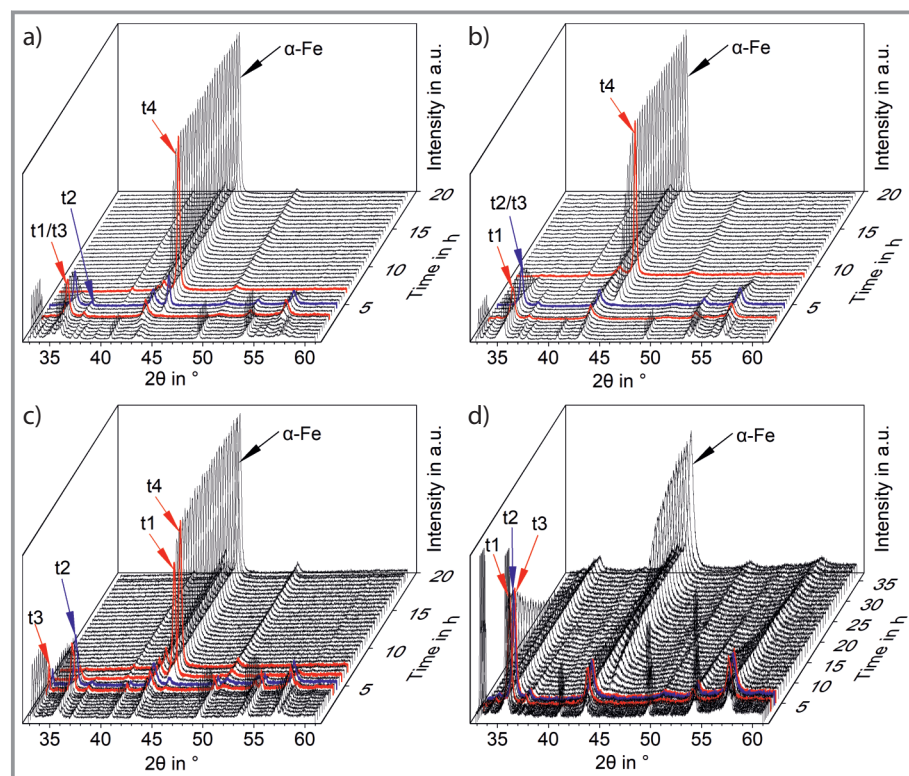


Figure 2. In situ X-ray diffractograms of the catalysts taken during the reduction process. a) 100Fe15Cu5K, b) 100Fe15Cu5K5Zn, c) 100Fe15Cu5K12Si, and d) 100Fe15Cu5K12Al, measurements were taken at 30, 100, 150, 200, 250, 300, and then continuously at 350 °C (t1, Fe₂O₃ vanishes; t2, gas change from 12 % H₂ in N₂ to 100 % H₂; t3, α -Fe emerges; t4, the iron is fully reduced).

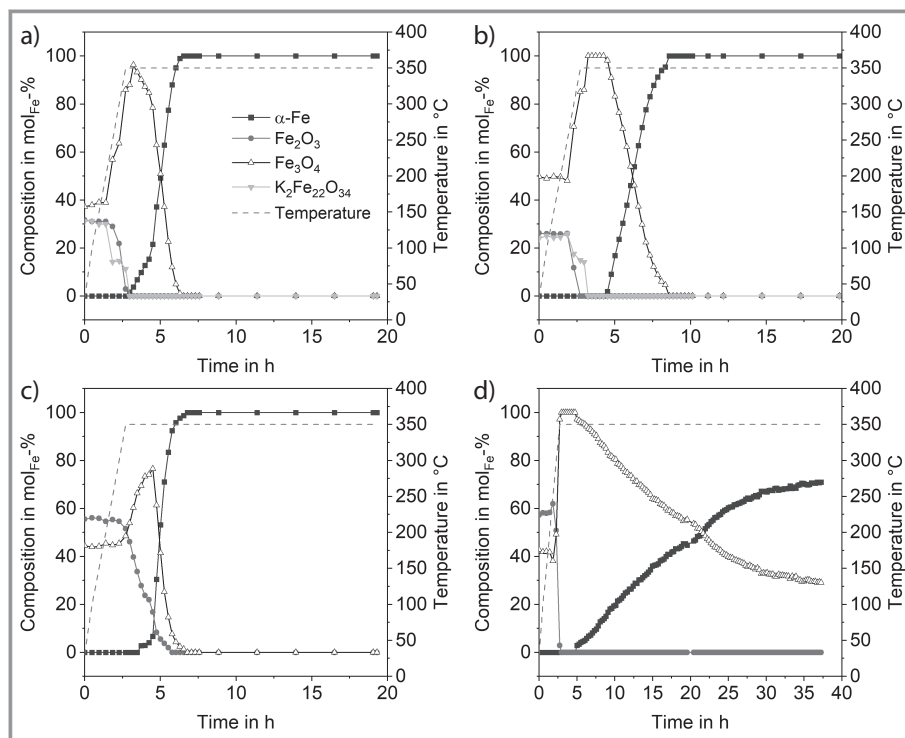


Figure 3. Composition of different iron species during reduction of different catalysts a) 100Fe15Cu5K, b) 100Fe15Cu5K5Zn, c) 100Fe15Cu5K12Si, and d) 100Fe15Cu5K12Al.

first completely converted into Fe_3O_4 , then followed by further reduction into $\alpha\text{-Fe}$, whereas for the catalyst 100Fe15Cu5K12Si, $\alpha\text{-Fe}$ started to form before Fe_2O_3 was fully reduced to Fe_3O_4 . In the reduced catalysts 100Fe15Cu5K, 100Fe15Cu5K5Zn, and 100Fe15Cu5K12Si, the iron phase consisted of 100 mol_{Fe}% $\alpha\text{-Fe}$. In the reduced catalyst 100Fe15Cu5K12Al, 70 mol_{Fe}% of $\alpha\text{-Fe}$ and 30 mol_{Fe}% of FeAl_2O_4 were found.

The crystallite sizes of the different iron species, obtained by Rietveld refinement, during reduction of all catalysts are shown in Fig. S2. In all the fresh catalysts, the crystallite size of Fe_2O_3 is much larger than the crystallite size of Fe_3O_4 . According to Fig. S2a, the crystallite size of Fe_2O_3 in 100Fe15Cu5K decreased from approx. 200 to 50 nm after 3 h. The crystallite size of Fe_2O_3 of 100Fe15Cu5K5Zn and 100Fe15Cu5K12Al catalysts initially was approx. 160 nm and then decreased to approx. 85 nm after about 3 h, as shown in Figs. S2b and S2d. Meanwhile, the crystallite size of Fe_2O_3 in the 100Fe15Cu5K12Si catalyst initially was 90 nm and then decreased to 40 nm after 5.5 h, as shown in Fig. S2c. The Fe_3O_4 crystallite size of 100Fe15Cu5K increased from 7 to 20 nm, whereas the Fe_3O_4 crystallite size of the 100Fe15Cu5K5Zn and 100Fe15Cu5K12Si catalysts shrank from 30 and 46 nm, respectively, to approx. 20 nm. Besides, the $\text{Fe}_3\text{O}_4/\text{FeAl}_2\text{O}_4$ crystallite size of 100Fe15Cu5K12Al catalyst decreased from 20 to 10 nm. On the contrary, the crystallite size of formed $\alpha\text{-Fe}$ grew during the reduction process. When the iron species were fully reduced, the $\alpha\text{-Fe}$ crystallite size did not change any longer.

Comparison of the initial Fe_2O_3 and Fe_3O_4 crystallite size in the fresh catalysts shows that adding structural promoters (ZnO , SiO_2 , and Al_2O_3) can reduce the crystallite size of Fe_2O_3 and increase the crystallite size of Fe_3O_4 in the fresh catalyst. Thereby, SiO_2 has the highest effect on the crystallite size change of the fresh catalyst. In addition, adding SiO_2 and Al_2O_3 as promoters can reduce the crystallite size of formed $\alpha\text{-Fe}$ in the reduced catalysts and adding ZnO as promoter has hardly any effect on the crystallite size of formed $\alpha\text{-Fe}$ in the reduced catalyst.

3.3 In Situ X-Ray Diffraction of Fischer-Tropsch Synthesis Reaction

The phase transformation of all four catalysts during FTS reaction under H_2/CO (= 2:1 (v/v)) at 220 °C and 9 bar were also investigated using in situ XRD. The in situ X-ray diffractograms are shown in Fig. S3. During the reaction, the $\alpha\text{-Fe}$ in the catalysts changed rapidly to iron carbide phases in the first few hours and afterwards, the formed iron carbide phases were stable without change. The X-ray diffractograms of the catalysts in the steady state, after 20 h of reaction, with PDF card information of the iron carbides can be found in Fig. S4. Characteristic XRD patterns of Fe_2C and Fe_5C_2 were identified for all the catalysts. For the catalyst 100Fe15Cu5K12Al, besides Fe_2C and Fe_5C_2 , a pattern characteristic for FeAl_2O_4 was also observed. In addition, a Rietveld refinement of the X-ray diffractogram of the catalyst 100Fe15Cu5K5Zn after 20 h of reaction is shown in Fig. S5 as an example. As can be observed in Fig. S5, both diffractograms, the observed one and the calculated one, are in good agreement.

Fig. 4 shows the composition of different iron phases obtained by Rietveld refinement of the corresponding diffractograms during FTS reaction. The graphs in the upper right corner of each graph show the change in the first 10 h. The reaction started with heating from 30 to 220 °C in 55 min. As can be seen in Fig. 4, as the temperature reached 220 °C, the $\alpha\text{-Fe}$ phase content dramatically declined for all catalysts. Meanwhile, $\epsilon\text{-Fe}_2\text{C}$ formed after 55 min of reaction followed by the formation of $\chi\text{-Fe}_5\text{C}_2$ after around 2 h of reaction. After several hours on stream, no $\alpha\text{-Fe}$ was found. For all catalysts, except 100Fe15Cu5K12Al, only two iron phases were found: $\epsilon\text{-Fe}_2\text{C}$ and $\chi\text{-Fe}_5\text{C}_2$, as illustrated in Figs. 4a to 4c. As shown in Fig. 4d, in case of the

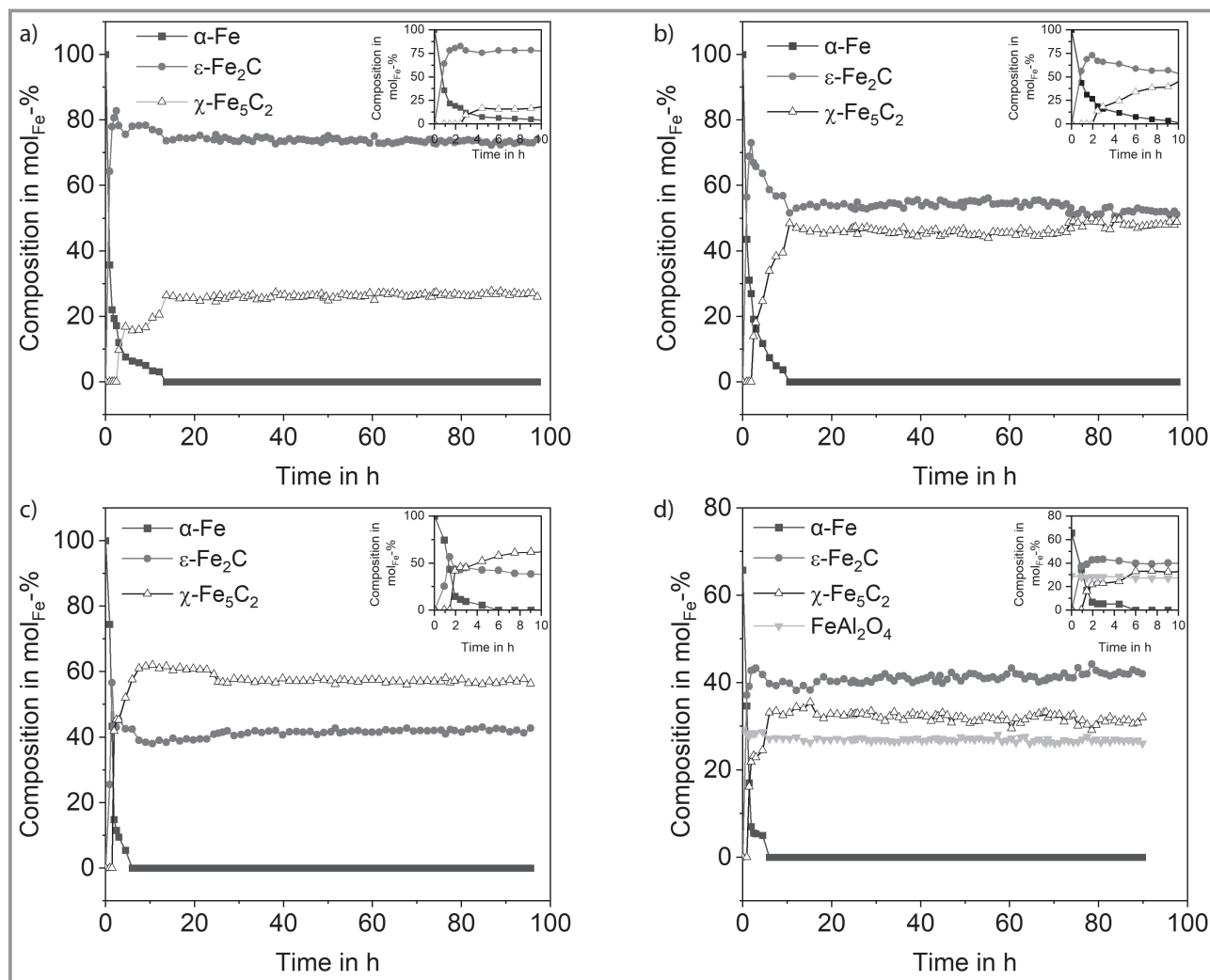


Figure 4. Composition of different iron species during FTS reaction under H_2/CO (= 2:1 (v/v)) at 220 °C and 9 bar of different catalysts a) 100Fe15Cu5K, b) 100Fe15Cu5K5Zn, c) 100Fe15Cu5K12Si, and d) 100Fe15Cu5K12Al.

100Fe15Cu5K12Al catalyst, besides $\epsilon\text{-Fe}_2\text{C}$ and $\chi\text{-Fe}_5\text{C}_2$, the barely changed FeAl_2O_4 is also present, which indicates that FeAl_2O_4 cannot be carburized at 220 °C and 9 bar under syngas. It turns out that once the $\alpha\text{-Fe}$ is fully carburized, the formed content of $\epsilon\text{-Fe}_2\text{C}$ and $\chi\text{-Fe}_5\text{C}_2$ only changed very slightly, which indicates that the carburization process of $\alpha\text{-Fe}$ is finished. For the 100Fe15Cu5K catalyst, the carburization process lasted 13 h as shown in Fig. 4a. The carburization process was 10 h for the 100Fe15Cu5K5Zn catalyst and 6 h for 100Fe15Cu5K12Si and 100Fe15Cu5K12Al (Figs. 4b–4d), respectively. This indicates that the addition of structural promoters (ZnO, SiO_2 , and Al_2O_3) accelerates the carburization process of iron-based catalysts. After the carburization process, in steady state, the $\epsilon\text{-Fe}_2\text{C}$ and $\chi\text{-Fe}_5\text{C}_2$ contents in 100Fe15Cu5K catalyst were 73 mol_{Fe}% and 27 mol_{Fe}%, respectively. In the structure-promoted catalysts 100Fe15Cu5K5Zn, 100Fe15Cu5K12Si, and 100Fe15Cu5K12Al, the $\epsilon\text{-Fe}_2\text{C}$ and $\chi\text{-Fe}_5\text{C}_2$ contents are 55 and 45 mol_{Fe}%, 43 and 57 mol_{Fe}%, 42 and 32 mol_{Fe}%,

respectively. The iron carbide compositions at steady state show that all catalysts with structural promoters (ZnO, SiO_2 , and Al_2O_3) favor the formation of $\chi\text{-Fe}_5\text{C}_2$, and the effect follows the order of $\text{SiO}_2 > \text{ZnO} > \text{Al}_2\text{O}_3$.

The crystallite sizes of different iron species during the FTS reaction of all the catalysts are shown in Fig. S6. The $\alpha\text{-Fe}$ crystallite size of all the catalysts decreased rapidly during the heating process at the beginning of the FTS reaction and then increased slightly. The crystallite size of formed $\epsilon\text{-Fe}_2\text{C}$ and $\chi\text{-Fe}_5\text{C}_2$ phases increased a bit during the carburization process and then stayed constant. The crystallite sizes of formed $\epsilon\text{-Fe}_2\text{C}$ and $\chi\text{-Fe}_5\text{C}_2$ at steady state are correlated to the crystallite size of $\alpha\text{-Fe}$ in the reduced catalysts: the larger the crystallite size of $\alpha\text{-Fe}$ in the reduced catalyst, the larger the crystallite size of iron carbides at steady state in the reacted catalyst. The crystallite size of FeAl_2O_4 in 100Fe15Cu5K12Al catalyst hardly changed during the reaction, which also shows that FeAl_2O_4 cannot be carburized under the given conditions.

3.4 Fischer-Tropsch Synthesis Reaction Performance

The FTS performance of 100Fe15Cu5K, 100Fe15Cu5K5Zn, 100Fe15Cu5K12Si, and 100Fe15Cu5K12Al catalysts was investigated in the lab-scale reactor setup shown in Fig. S1. All the catalysts were first reduced with the same reduction procedure as for the in situ XRD. After reduction, the FT reaction at 220 °C, 9 bar and H₂/CO (= 2:1 (v/v)) was started, also analogous to the in situ XRD measurements. The FTS activity of all the catalysts in terms of reaction rate is shown in Fig. 5. The reaction rate of 100Fe15Cu5K decreased within the 95-h time on stream. On the contrary, for all catalysts with a structure promoter, a short induction period was observed and then a steady state was achieved after approx. 5 h under reaction conditions at 220 °C. This indicates that the addition of structural promoters (ZnO, SiO₂, and Al₂O₃) stabilizes the FTS catalyst, possibly by preventing coke formation, as no change in the bulk of the catalyst could be seen in XRD. The short induction period is probably due to carburization of α -Fe into the iron carbides as proved by in situ XRD. Although the reaction rate of 100Fe15Cu5K kept dropping from $2.3 \cdot 10^{-6}$ to $1.75 \cdot 10^{-6}$ mol_{CO}g_{Fe}⁻¹s⁻¹, it still shows the highest rate among all investigated catalysts. For the three catalysts with a structure promoter, at the steady state of the FTS reaction, the 100Fe15Cu5K5Zn catalyst shows the highest rate of $1.3 \cdot 10^{-6}$ mol_{CO}g_{Fe}⁻¹s⁻¹, which is 4 times higher compared to the 100Fe15Cu5K12Al catalyst ($3.2 \cdot 10^{-7}$ mol_{CO}g_{Fe}⁻¹s⁻¹). Besides, 100Fe15Cu5K12Si catalysts showed an intermediate rate of $9.7 \cdot 10^{-6}$ mol_{CO}g_{Fe}⁻¹s⁻¹, 3 times higher than that of the 100Fe15Cu5K12Al catalyst. The rate of the catalysts is correlated to the ϵ -Fe₂C amount in the catalysts at stable state: As shown in Fig. 3, the ϵ -Fe₂C amount follows the order 100Fe15Cu5K (73 mol_{Fe} %) > 100Fe15Cu5K5Zn (55 mol_{Fe} %) > 100Fe15Cu5K12Si (43 mol_{Fe} %) > 100Fe15Cu5K12Al (42 mol_{Fe} %), which is also the order of the rate. This indicates that, compared to the χ -Fe₅C₂ phase, ϵ -Fe₂C is the more active phase in the FTS reaction. This was also found by Lu et al. [19], who stated that ϵ -Fe₂C is more responsible for FTS activity. Besides this aspect, the relative low reaction rate of the 100Fe15Cu5K12Al catalyst is due to the FeAl₂O₄ phase, which is believed not to be active for FTS. The difference in specific surface area proba-

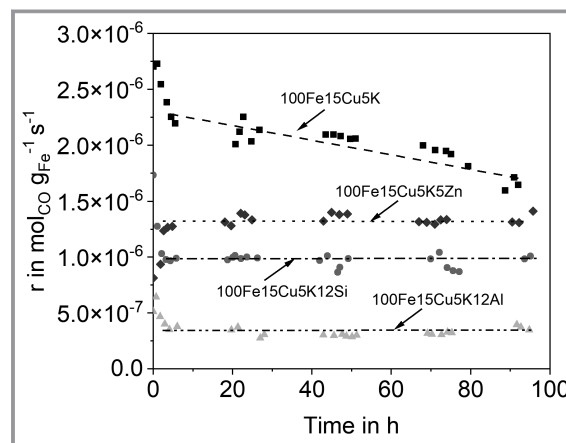


Figure 5. Reaction rate of FTS reaction for catalysts 100Fe15Cu5K, 100Fe15Cu5K5Zn, 100Fe15Cu5K12Si, and 100Fe15Cu5K12Al (reaction conditions: H₂/CO = 2, 220 °C, 9 bar, 20 L_{STP}h⁻¹, *m*_{cat} = 7.5 g).

bly is not the reason for the different activity of the catalysts, as the surface area of the reduced catalysts is roughly inversely proportional to the activity (Tab. 1).

The selectivity towards CO₂ and hydrocarbons and the ratio between ϵ -Fe₂C/ χ -Fe₅C₂, which is obtained from the in situ XRD results, are shown in Tab. 3. The 100Fe15Cu5K catalyst has the highest CO₂ selectivity of 24.7 wt_C %. It is followed by the 100Fe15Cu5K5Zn and 100Fe15Cu5K12Al catalysts, both of which have a CO₂ selectivity of approx. 22 wt_C %, which is twice as high as the CO₂ selectivity of the 100Fe15Cu5K12Si catalyst (11.2 wt_C %). The comparison of the CO₂ selectivity with respect to the ϵ -Fe₂C/ χ -Fe₅C₂ ratio shows that the higher the ϵ -Fe₂C/ χ -Fe₅C₂ of the catalyst, the higher the CO₂ selectivity, which indicates that the ϵ -Fe₂C phase favors the formation of CO₂, which matches well with the results of Wang et al. [20]. As shown in Tab. 3, the 100Fe15Cu5K has the lowest CH₄ selectivity of 6.4 wt_C %, followed by 100Fe15Cu5K5Zn and 100Fe15Cu5K12Al with a CH₄ selectivity of 7.7 and 9.3 wt_C %, respectively. The 100Fe15Cu5K12Si has the highest CH₄ selectivity of 13.6 wt_C %. Comparison with the ϵ -Fe₂C/ χ -Fe₅C₂ ratio shows that χ -Fe₅C₂ favors the formation of CH₄. The selectivity towards C₂-C₄ shows a similar trend. Among all catalysts, 100Fe15Cu5K,

Table 3. The CO₂ and hydrocarbon selectivity in FTS and iron carbides ratio of different iron-based catalysts.

Catalyst	CO ₂ selectivity, [wt _C %]	Hydrocarbon selectivity [wt _C %]			ϵ -Fe ₂ C/ χ -Fe ₅ C ₂ ^{a)}
		CH ₄	C ₂ -C ₄	C ₅₊	
100Fe15Cu5K	24.7	6.4	30.0	63.6	3.5
100Fe15Cu5K5Zn	21.6	7.7	26.7	65.6	1.2
100Fe15Cu5K12Si	11.2	13.6	47.1	39.3	0.8
100Fe15Cu5K12Al	22.2	9.3	35.4	55.3	1.3

a) Data from the in situ XRD under reaction conditions at steady state.

100Fe15Cu5K5Zn, and 100Fe15Cu5K12Al have a relatively low C₂–C₄ selectivity of 30, 26.7, and 35.4 wt_C %, respectively. The catalyst 100Fe15Cu5K12Si with the lowest ε -Fe₂C/ χ -Fe₅C₂ ratio has the highest C₂–C₄ selectivity of 47.1 wt_C %, which indicates that the χ -Fe₅C₂ phase benefits the formation of C₂–C₄ in the FTS reaction or lowers the chain growth probability. Accordingly, the 100Fe15Cu5K, 100Fe15Cu5K5Zn, and 100Fe15Cu5K12Al catalysts show a higher C₅₊ selectivity and the 100Fe15Cu5K12Si shows the lowest C₅₊ selectivity. As the C₅₊ selectivity of the catalysts roughly correlates with the ε -Fe₂C/ χ -Fe₅C₂ ratio, it is believed that the ε -Fe₂C phase is in favor of forming C₅₊ products.

4 Conclusions

In this work, an in situ XRD approach was used to investigate the influence of ZnO, SiO₂, and Al₂O₃ as structural promoters during reduction and reaction of iron-based FTS catalysts. Additionally, the FTS performance of all the catalysts was studied in a fixed-bed reactor to clarify the role of different iron carbides. Based on in situ XRD results for the reduction of the catalysts, it is concluded that all the iron-based catalysts follow the same sequential reduction pathway of Fe₂O₃/K₂Fe₂₂O₃₄ → Fe₃O₄ → α -Fe during the reduction by H₂ at 350 °C, except for FeAl₂O₄, which is not reducible at the given conditions, as observed in the 100Fe15Cu5K12Al catalyst. Besides, the reduction process was delayed and prolonged by the presence of ZnO, SiO₂, and Al₂O₃. It is found from the in situ XRD results during FTS that all the iron-based catalysts formed ε -Fe₂C and χ -Fe₅C₂ and that FeAl₂O₄ cannot be reduced or carburized under the used reaction conditions. In addition, the carburization process was accelerated and the formation of χ -Fe₅C₂ was favored by the existence of ZnO, SiO₂, and Al₂O₃. During the FTS reaction, the reaction rate of 100Fe15Cu5K decreased, but the presence of ZnO, SiO₂, and Al₂O₃ stabilized the reaction rate and prevented deactivation. Furthermore, the different activity of catalysts shows that, compared to χ -Fe₅C₂, ε -Fe₂C seems to be a more active phase. The selectivity of CO₂ and hydrocarbons in the FTS reaction indicates that ε -Fe₂C favors the formation of CO₂ and C₅₊, whereas χ -Fe₅C₂ benefits the formation of CH₄ and C₂–C₄ products.

In summary, a combination of in situ XRD and fixed-bed reactor were used in this work to investigate the correlations between the catalytic performance and iron carbides, providing a better understanding of the role of the ZnO, SiO₂, and Al₂O₃ in formation of different iron carbides and in the FTS reaction.

Supporting Information

Supporting Information for this article can be found under DOI: <https://doi.org/10.1002/cite.202200056>.

The authors are indebted to the German Research Foundation (DFG) for financial support of the project DFG Je 257/26-1. Open access funding enabled and organized by Projekt DEAL.

Symbols used

\dot{m}	[kg s ⁻¹]	mass flow
\dot{n}	[mol s ⁻¹]	molar flow
r	[mol _{CO} g _{Fe} ⁻¹ s ⁻¹]	reaction rate
S	[-]	selectivity
t	[h]	time

Sub- and superscripts

C	carbon
cat	catalyst
CO	carbon monoxide
CO ₂	carbon dioxide
n	compound n
STP	IUPAC standard temperature and pressure (273.15 K, 1 bar)

Abbreviations

FTS	Fischer-Tropsch synthesis
GC	gas chromatography
ICP-OES	inductively coupled plasma optical emission spectroscopy
WGS	water gas shift
XRD	X-ray diffraction

References

- [1] A. Jess, P. Wasserscheid, *Chemical Technology*, 2nd ed., Wiley-VCH, Weinheim **2020**.
- [2] M. E. Dry, The Fischer-Tropsch Synthesis, in *Catalysis Science and Technology* (Eds: J. R. Anderson, M. Boudart), Springer, Berlin **1981**.
- [3] B. Jager, *Developments in Fischer-Tropsch Technology*, in *Studies in Surface Science and Catalysis* (Eds: M. de Pontes, R. L. Espinoza, C. P. Nicolaides, J. H. Scholtz, M. S. Scurrell), Vol. 107, Elsevier, Amsterdam **1997**.
- [4] C. Frohning, W. Rottig, F. Schnur, *Chemierohstoffe aus Kohle*, Georg Thieme, Stuttgart **1977**.
- [5] R. B. Anderson, H. Köbel, M. Rálek, *The Fischer-Tropsch Synthesis*, Academic Press, Orlando, FL **1984**.

- [6] E. de Smit, B. M. Weckhuysen, *Chem. Soc. Rev.* **2008**, *37* (12), 2758–2781. DOI: <https://doi.org/10.1039/b805427d>
- [7] H. Hayakawa, H. Tanaka, K. Fujimoto, *Appl. Catal., A* **2006**, *310*, 24–30. DOI: <https://doi.org/10.1016/j.apcata.2006.04.045>
- [8] E. de Smit, A. M. Beale, S. Nikitenko, B. M. Weckhuysen, *J. Catal.* **2009**, *262* (2), 244–256. DOI: <https://doi.org/10.1016/j.jcat.2008.12.021>
- [9] R. J. O'Brien, B. H. Davis, *Catal. Lett.* **2004**, *94* (1–2), 1–6. DOI: <https://doi.org/10.1023/B:CATL.0000019322.69160.ef>
- [10] S. Li, A. Li, S. Krishnamoorthy, E. Iglesia, *Catal. Lett.* **2001**, *77*, 197–205. DOI: <https://doi.org/10.1023/A:1013284217689>
- [11] J. Li, X. Cheng, C. Zhang, J. Wang, W. Dong, Y. Yang, Y. Li, *J. Chem. Technol. Biotechnol.* **2017**, *92* (6), 1472–1480. DOI: <https://doi.org/10.1002/jctb.5152>
- [12] *Fischer-Tropsch Technology* (Eds: A. P. Steynberg, M. E. Dry), Studies in Surface Science and Catalysis, Vol. 152, Elsevier, Amsterdam **2004**.
- [13] W. Ngantsoue-Hoc, Y. Zhang, R. J. O'Brien, M. Luo, B. H. Davis, *Appl. Catal., A* **2002**, *236* (1–2), 77–89. DOI: [https://doi.org/10.1016/S0926-860X\(02\)00278-8](https://doi.org/10.1016/S0926-860X(02)00278-8)
- [14] D. B. Bukur, W.-P. Ma, V. Carreto-Vazquez, *Top. Catal.* **2005**, *32* (3–4), 135–141. DOI: <https://doi.org/10.1007/s11244-005-2885-6>
- [15] H. Wan, B. Wu, C.-H. Zhang, H. Xiang, Y. Li, B.-F. Xu, F. Yi, *Catal. Commun.* **2007**, *8* (10), 1538–1545. DOI: <https://doi.org/10.1016/j.catcom.2007.01.002>
- [16] X. Gao, J. Zhang, N. Chen, Q. Ma, S. Fan, T. Zhao, N. Tsubaki, *Chin. J. Catal.* **2016**, *37* (4), 510–516. DOI: [https://doi.org/10.1016/S1872-2067\(15\)61051-8](https://doi.org/10.1016/S1872-2067(15)61051-8)
- [17] H. Suo, S. Wang, C. Zhang, J. Xu, B. Wu, Y. Yang, H. Xiang, Y. Li, *J. Catal.* **2012**, *286*, 111–123. DOI: <https://doi.org/10.1016/j.jcat.2011.10.024>
- [18] H. Wan, B. Wu, T. Li, Z. Tao, X. An, H. Xiang, Y. Li, *J. Fuel Chem. Technol.* **2007**, *35* (5), 589–594. DOI: [https://doi.org/10.1016/S1872-5813\(07\)60036-X](https://doi.org/10.1016/S1872-5813(07)60036-X)
- [19] F. Lu, X. Chen, Z. Lei, L. Wen, Y. Zhang, *Appl. Catal., B* **2021**, *281*, 119521. DOI: <https://doi.org/10.1016/j.apcatb.2020.119521>
- [20] P. Wang, W. Chen, F. K. Chiang, A. I. Dugulan, Y. J. Song, R. Pestman, K. Zhang, J. S. Yao, B. Feng, P. Miao, W. Xu, E. J. M. Hensen, *Sci. Adv.* **2018**, *4* (10), eaau2947. DOI: <https://doi.org/10.1126/sciadv.aau2947>